J Comput Neurosci
DOI 10.1007/s10827-009-0167-1

Variability of bursting patterns in a neuron model in the presence of noise

Paul Channell · Ibiyinka Fuwape · Alexander B. Neiman · Andrey L. Shilnikov

Received: 13 May 2008 / Revised: 8 May 2009 / Accepted: 29 May 2009

Abstract Spiking and bursting patterns of neurons are characterized by a high degree of variability. A single neuron can demonstrate endogenously various bursting patterns, changing in response to external disturbances due to synapses, or to intrinsic factors such as channel noise. We argue that in a model of the leech heart interneuron existing variations of bursting patterns are significantly enhanced by a small noise. In the absence of noise this model shows periodic bursting with fixed numbers of interspikes for most parameter values. As the parameter of activation kinetics of a slow potassium current is shifted to more hyperpolarized values of the membrane potential, the model undergoes a sequence of incremental spike adding transitions accumulating towards a periodic tonic spiking activity. Within a narrow parameter window around every spike adding transition, spike alteration of bursting is deterministically chaotic due to homoclinic bifurcations of a saddle periodic orbit. We have found that near these transitions the interneuron model becomes extremely sensitive to small random perturbations that cause a wide expansion and overlapping of the chaotic windows. The chaotic behavior is characterized by positive values of the largest Lyapunov exponent, and of the Shannon entropy of probability distribution of spike numbers per burst. The windows of chaotic dynamics resemble the Arnold tongues being plotted in the parameter plane, where the noise intensity serves as a second control parameter. We determine the critical noise intensities above which the interneuron model generates only irregular bursting within the overlapped windows.

Keywords Bursting · Noise · Neuron · Model · Chaos · Transition · Entropy · Lyapunov exponent · Homoclinic · Bifurcation · Spiking · Adding · Pattern

Action Editor: J. Rinzel

P. Channell · A. L. Shilnikov (✉)
Department of Mathematics and Statistics,
Georgia State University, Atlanta,
GA 30303, USA
e-mail: ashilnikov@gsu.edu

I. Fuwape · A. B. Neiman
Department of Physics and Astronomy,
Ohio University, Athens, OH
45701, USA

A. B. Neiman
e-mail: neimana@ohio.edu

I. Fuwape
Department of Physics, Federal University
of Technology, Akure, PMB 704, Nigeria

A. L. Shilnikov
The Neuroscience Institute,
Georgia State University, Atlanta, GA
30303, USA

1 Introduction

Most networked neurons demonstrate oscillations of the membrane potential either endogenously or due to external perturbations. Bursting is a manifestation of the slow–fast dynamics observed in neuroscience (Izhikevich 2007; Steriade et al. 1990; Cymbalyuk et al. 2002). The functional role of bursting has been the focus of various theoretical and experimental studies.

Published online: 20 June 2009

Bursting on various time scales has been discovered in pathological brain states (Steriade et al. 1993), while Marder and Calabrese (1996) reveals its importance for rhythmicity of central pattern generators controlling motor behavior (Kopell 1988).

Deterministic description of *endogenous* oscillatory activities, such as tonic spiking and bursting, in neuronal dynamics is based on the examination of generic properties of various mathematic models, in particular realistic ones derived through the Hodgkin-Huxley formalism (Hodgkin and Huxley 1952). A typical neuronal model falls into a special class of dynamical systems with at least two distinct time scales, the so-called slow–fast systems (Rinzel 1985; Rinzel and Ermentrout 1998; Rinzel and Wang 1995; Jones and Kopell 1994; Arnold et al. 1994; Bertram et al. 1995; Izhikevich 2000). Using the transparent geometric methods based on the dissection of such a slow-fast system, one can detect and follow the branches of equilibria and limit cycles in the fast subsystem. Dynamics of a singularly perturbed system are then determined by and centered around the corresponding attracting segments of these slow motion manifolds of its fast subsystem (Tikhonov 1948; Pontryagin and Rodygin 1960; Fenichel 1979; Jones and Kopell 1994). A neuron model possesses a pair of such manifolds called quiescent and tonic spiking, respectively.

Geometrical configurations for slow-fast neuron models pioneered by Rinzel (Rinzel 1985; Rinzel and Ermentrout 1998; Rinzel and Wang 1995), and further enhanced in Bertram et al. (1995), Guckenheimer (1996), Izhikevich (2000, 2007) give the classification schemes for bursting based on planer bifurcations which initiate or terminate fast trajectory transitions between the slow-motion manifolds in the phase space of the neuron model. They work exceptionally well in the most low-order mathematical and realistic models far from bifurcations of bursting. However, at activity transitions, the bursting behavior can become drastically complex and even chaotic (Terman 1991, 1992; Holden and Fan 1992; Wang 1993; Belykh et al. 2000; Feudel et al. 2000; Deng and Hines 2002; Elson et al. 2002; Shilnikov and Cymbalyuk 2004; Cymbalyuk and Shilnikov 2005; Channell et al. 2007a) due to reciprocal interaction between the slow and fast dynamics, which lead to the emergence of novel dynamical phenomena and bifurcations that can *only* occur in the entire system. Recently a novel method which identifies effective low-dimensional local models to study the transition between tonic and bursting regimes was developed in Clewley et al. (2009). However, the current description of transition routes between tonic spiking and bursting activities is still incomplete. There have been a few such bifurcation scenarios based on the nonlocal bifurcation theory. The first generic mechanism leading to the emergence of the square wave bursters (Rinzel 1985) from tonic spiking through a homoclinic bifurcation in a subsystem of the model was analyzed rigorously in Terman (1991); chaotic dynamics at the transition is its key signature. The breakthrough in this direction came in recently with the discovery of two novel transitions occurring at the loss of stability of a tonic spiking periodic orbit though the homoclinic saddle-node bifurcation of periodic orbits. The first transition, reversible and continuous, which occurs in the reduced model of the leech heart interneuron (Shilnikov and Cymbalyuk 2004, 2005) and in a modified Hindmarsh-Rose model of square-wave burster (Shilnikov and Kolomiets 2008), is based on the blue sky catastrophe (Shilnikov et al. 1998, 2001). The feature of the second transition mechanism is the bi-stability of the co-existing tonic spiking and bursting in a neuron model (Shilnikov and Cymbalyuk 2004; Shilnikov et al. 2005). Another feature of this bifurcation is transient chaos where the neuron generates an unpredictable number of burst trains before it starts spiking tonically. The most recent transition mechanics in this line is generic for Fold-Fold and elliptic burster models of neurons: it describes the onset of bursting through the breakdown of a canard invariant torus at the fold of the tonic spiking manifold of a model, so that transient modulations of tonic spiking voltage traces are its evidently signature (Kramer et al. 2008).

Studies of bursting and its transformations in neuronal models require a non-local bifurcation analysis, which is based on the Poincaré return mappings (Shilnikov et al. 1998, 2001). Return mappings have been actively used in computational neuroscience, see Chay (1985), Holden and Fan (1992), Medvedev (2006), Shilnikov and Rulkov (2003, 2004) and references therein. A drawback of mappings constructed from time series is in their sparseness, as they reflect only dominating attractors of a system. In some cases, feasible reductions to one or two dimensional mappings can be achieved through slow–fast scale decomposition of the phase variables (Medvedev 2005; Shilnikov and Kolomiets 2008; Griffiths and Pernarowski 2006). A novel practical method for constructing a complete family of *onto* mappings for membrane potentials of slow-fast neuronal models was proposed in Channell et al. (2007a, b) following an idea suggested originally in Shilnikov (1993). Using this approach we have studied spike adding transitions in a leech heart interneuron model and revealed that this phenomenon is associated with homoclinic bifurcations of a saddle periodic orbit (Channell et al. 2007a).

In general, chaos in slow–fast systems is an atypical phenomenon as it takes place mainly near transitions between tonic spiking and bursting (Terman 1991, 1992; Wang 1993; Belykh et al. 2000; Cymbalyuk and Shilnikov 2005; Feudel et al. 2000; Deng and Hines 2002). Indeed, robust regular dynamics of slow–fast neuron models contrast to that of real isolated bursting neurons exhibiting time dependent variability of oscillatory patterns. However, pure deterministic modeling is incomplete as noise is inevitably present in any dissipative physical system. Several sources of randomness were identified in neural systems (Manwani and Koch 1999), including ion channel noise (Chow and White 1996), and synaptic noise. Noise can significantly modify deterministic neuronal dynamics leading to more regular regimes with negative Lyapunov exponent reflected in enhanced spike timing reliability (Mainen and Sejnowski 1995; Goldobin and Pikovsky 2005). On the other hand, channel or synaptic noise may result in irregular dynamics with positive Lyapunov exponent (Rowat and Elson 2004; Carelli et al. 2005; Goldobin and Pikovsky 2006).

In this paper we study spike adding bifurcations of bursting patterns in a simplified model of the leach heart interneuron. When isolated pharmacologically from a leech heartbeat central pattern generator, an individual interneuron shows an autonomous bursting behavior (Cymbalyuk et al. 2002). A detailed biophysical model (Hill et al. 2001) was simplified in Cymbalyuk and Calabrese (2001) and successfully used to study fundamental bifurcation mechanisms of bursting regimes in Cymbalyuk and Calabrese (2001), Shilnikov and Cymbalyuk (2005), Shilnikov et al. (2005), Channell et al. (2007a). Although spike adding transitions were observed and studied in the Chay and Hindmarsh–Rose mathematical models before (Chay 1985; Fan and Holden 1995; Gu et al. 2002; Yang et al. 2006), the mechanism of spike adding bifurcations in the interneuron model under consideration is very distinct. First, we review the deterministic mechanism of this transition. Next, we consider the influence of random synaptic current with the aim to show that addition of noise is necessary to account for variability observed in experimental studies of real neurons and neural networks.

2 Deterministic dynamics

2.1 Interneuron model

A reduced model of the leach heart interneuron is given by the following set of three nonlinear coupled differential equations (Cymbalyuk and Calabrese 2001; Shilnikov and Cymbalyuk 2005; Shilnikov et al. 2005; Channell et al. 2007a):

$$
\begin{aligned}
&C\frac{dV}{dt} = -I_{\mathrm{Na}} - I_{\mathrm{K2}} - I_{\mathrm{L}} + I_{\mathrm{app}},\\
&I_L = \bar{g}_{\mathrm{L}}\,(V - E_{\mathrm{L}}), \quad I_{\mathrm{K2}} = \bar{g}_{\mathrm{K2}}\, m_{\mathrm{K2}}^2 (V - E_{\mathrm{K}}),\\
&I_{\mathrm{Na}} = \bar{g}_{\mathrm{Na}}\, m_{\mathrm{Na}}^3\, h_{\mathrm{Na}}\,(V - E_{\mathrm{Na}}),\\
&\tau_{\mathrm{Na}}\frac{dh_{\mathrm{Na}}}{dt} = h_{\mathrm{Na}}^{\infty}(V) - h, \quad m_{\mathrm{Na}} = m_{\mathrm{Na}}^{\infty}(V),\\
&\tau_{\mathrm{K2}}\frac{dm_{\mathrm{K2}}}{dt} = m_{\mathrm{K2}}^{\infty}(V) - m_{\mathrm{K2}}.
\end{aligned}
\tag{1}
$$

Here, $C = 0.5$ nF is the membrane capacitance; V is the membrane potential in mV; I_{Na} is the sodium current with slow inactivation h_{Na} and fast activation m_{Na}; I_{K2} is the slow persistent potassium current with activation m_{K2}; I_{L} is the leak current and I_{app} is an applied current. The values of maximal conductances are set as $\bar{\mathrm{g}}_{\mathrm{K2}} = 30$ nS, $\bar{g}_{\mathrm{Na}} = 200$ nS and $\mathrm{g_L} = 8$ nS. The reversal potentials are $\mathrm{E_{Na}} = 45$ mV, $\mathrm{E_K} = -70$ mV and $E_{\mathrm{L}} = -46$ mV. The time constants of gating variables are $\tau_{\mathrm{K2}} = 0.25$ s and $\tau_{\mathrm{Na}} = 0.0405$ s. The steady state values of gating variables, $h_{\mathrm{Na}}^{\infty}(V)$, $m_{\mathrm{Na}}^{\infty}(V)$, $m_{\mathrm{K2}}^{\infty}(V)$, are given by the following Boltzmann equations,

$$
\begin{aligned}
&h_{\mathrm{Na}}^{\infty}(V) = [1 + \exp(0.5(V + 33.3))]^{-1}\\
&m_{\mathrm{Na}}^{\infty}(V) = [1 + \exp(-0.15(V + 30.5))]^{-1}\\
&m_{\mathrm{K2}}^{\infty}(V) = [1 + \exp\,(-0.083(V + 18 + \mathrm{V_{K2}^{shift}}))]^{-1}.
\end{aligned}
\tag{2}
$$

The intrinsic bifurcation parameter $\mathrm{V_{K2}^{shift}}$ of the model is a deviation from $V_{1/2} = 18$ mV corresponding to the half-activated potassium channel at $m_{\mathrm{K2}}^{\infty} = 1/2$. In the model (1), decreasing $\mathrm{V_{K2}^{shift}}$ elevates the slow nullcline $\frac{dm_{\mathrm{K2}}}{dt} = 0$ in the V-direction, thereby delaying the activation of m_{K2}. In this study, the range of the control parameter $\mathrm{V_{K2}^{shift}}$ is $[-26;\ 1.8]$ mV; the upper boundary of the interval corresponds to the hyperpolarized quiescent state of the neuron, whereas it fires tonically at the lower $\mathrm{V_{K2}^{shift}}$ values. In this study the applied current is zero for the deterministic case and is a zero-mean Gaussian noise for the stochastic case.

2.2 Spike adding cascade in bursting towards spiking

Bursting in the model (1) originates and evolves through a spike adding cascade as the bifurcation parameter shifts the half-activation potential of the slow potassium current towards more hyperpolarized values: the number of spikes per burst grows incrementally

with no bound until the interneuron model (1) starts to fire spikes continuously. The initial stages of the spike adding cascade are shown in Fig. 1. The spike adding begins at $V_{K2}^{shift} \simeq 8$ mV after the loss of stability of the stable hyperpolarized quiescent state of the neuron leading to the emergence of a single spike bursting. It continues until $V_{K2}^{shift} \simeq -24.828$ mV, beyond which the tonic spiking phase of bursting becomes of infinite length (Shilnikov et al. 2005; Channell et al. 2007a), i.e. transforms into tonic spiking. Every spike addition occurs within extremely narrow parameter window where the model shows a transient behavior resulting in generation of a series of bursts with an unpredictably changing number of spikes.

2.3 Onto Poincaré mapping near bursting manifold

Study of mechanisms of bursting and its transformations requires nonlocal bifurcation analysis, which is based on the derivation and further examination of Poincaré return mappings. Here, we first discuss a method of construction of one-dimensional Poincaré mapping and then examine such a mapping to elucidate the mechanism of spike adding bifurcations and the origin of dynamical chaos in the model. The discussed numerical technique of the mapping construction is broadly applicable to most slow-fast neuronal models. Observe that due to the disparity of the time scales of the phase variables, the model (1) can be treated within the framework of slow–fast systems. The ground stage in the construction of the mapping is to single out so-called slow motion manifolds, which correspond to the tonic spiking and quiescent manifolds in the computational neuroscience context. These manifolds, labeled M_{lc} and M_{eq} in Fig. 2, are comprised of the periodic orbits and equilibria of Eq. (1), respectively. Hence the fast subsystem is formed by the first two equations from the slow-fast decomposition paradigm. To locate the manifolds in the 3D phase space of the model, we used an approach proposed in Channell et al. (2007a, b). Its essence is the parameter continuation technique applied to the entire set of Eq. (1) rather than to its dissected fast subsystem. The advantage of our approach is that it yields the sought manifolds themselves in the phase space of the model rather than approximations of the manifold in a singular limit. This approach is especially valuable for neuronal models of higher dimensions where slow–fast dissections could be problematic because of multiple time scales for various ionic currents involved in the dynamics.

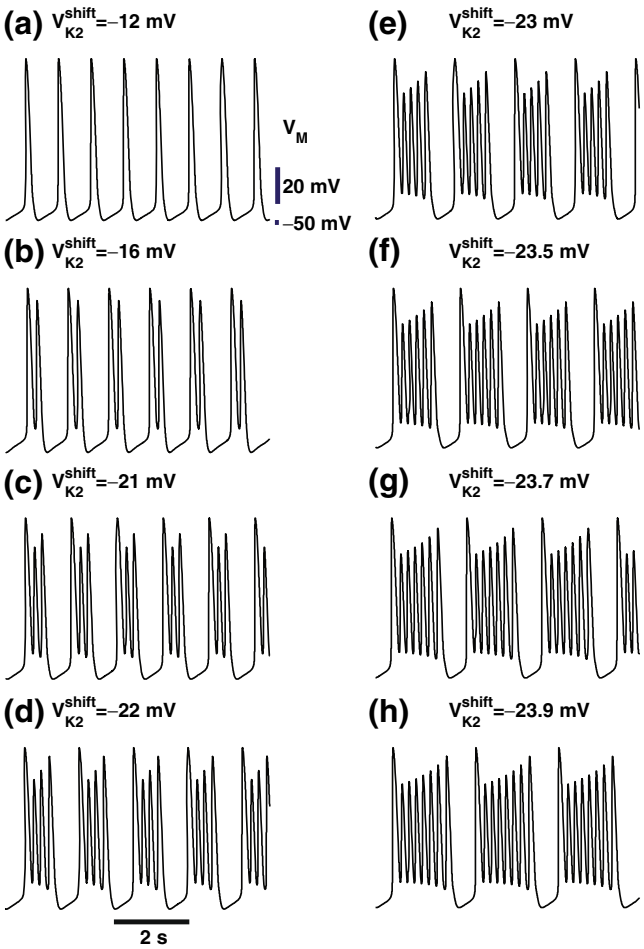

Fig. 1 Incremental spike adding cascade progresses in the interneuron model (1) as the parameter V_{K2}^{shift} is shifted towards more hyperpolarized potentials (**a**–**h**)

Figure 2 shows the parametric slow motion manifolds, tonic spiking M_{lc} and quiescent M_{eq}, and also illustrates the procedure of building the one-dimensional Poincaré mapping. To localize the tonic spiking manifold a stable periodic orbit is first detected in the phase space of the model: this small-amplitude orbit at $V_{K2}^{shift} = -26$ mV is the edge of the desired manifold M_{lc} in Fig. 2. Next, a branch of the periodic orbits is followed (using the software package CONTENT, ftp://ftp.cwi.nl/pub/CONTENT) as V_{K2}^{shift} is increased from −26 through 1.8 mV. Approaching the latter value, the stable manifold M_{lc} folds back, wraps around the quiescent manifold M_{eq} and touches its low hyperpolarized fold. We stress that revealing such a topology of the spiking manifold would be impossible with the slow–fast dissection (Cymbalyuk and Shilnikov 2005). Thus, by construction the aforementioned center manifold M_{lc} is a parametrically sought two-dimensional surface foliated by a large number of the spiking periodic orbits of the model (1). A solution of Eq. (1) repeatedly switching between M_{eq} and M_{lc} represents the busting activity. The hyperpolarized fold on M_{eq} corresponds

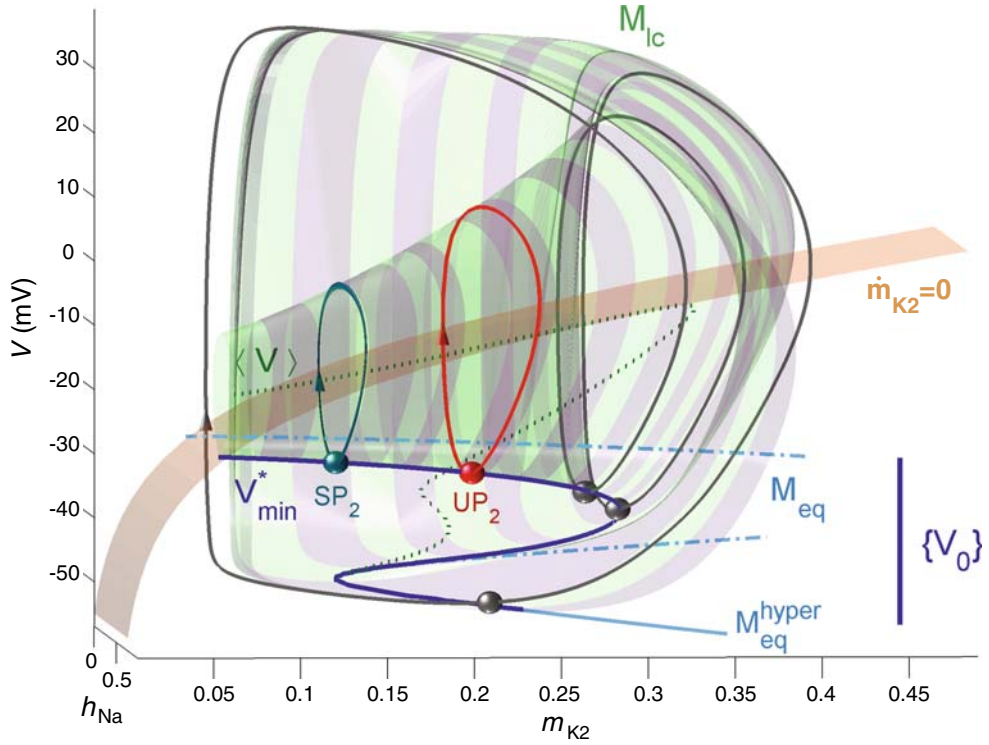

Fig. 2 (A) Slow motion manifolds and nullclines of the model (1): the 2D spiking manifold M_{lc} is foliated by the periodic orbits continued, from the *left* to the *right*, as the parameter V_{K2}^{shift} is increased from −26 through 1.8 mV. The space curves V^*_{min} and ⟨V⟩ are made of minimal and average coordinates of the periodic orbits. M_{lc} glues to the quiescent manifold, M_{eq}, comprised of the equilibrium states of Eq. (1), at its lower fold where the curve ⟨V⟩ terminates at. An equilibrium state of Eq. (1) resides at the intersection point of M_{eq} with the slow (*yellow*) nullcline $\dot{m}_{K2} = 0$ for given V_{K2}^{shift}. The set $\{V_0\}$ contains the V-minimal coordinated values of the periodic orbits M_{lc}. Thus selected points are used to generate the outgoing trajectories that define the Poincaré mapping taking V^*_{min} onto itself after one revolution around M_{lc}. An initial point returning after a single, or several turns around M_{lc} in itself, is a fixed (two balls UP_2 and SP_2) or a periodic point (three balls on the coexisting bursting orbit shown in grey) of the mapping, respectively

to the beginning of a burst. The number of complete revolutions of the solution around M_{lc} before it reaches the fold on the spiking manifold is the number of spikes per burst. We use this winding number to classify bursting regimes. Next, we construct numerically the onto mapping taking a voltage interval onto itself. This interval is comprised of the minimal values (denoted by V_0) of the membrane potentials found on the all detected periodic orbits that constitute the manifold M_{lc}. These minima form the space curve labeled V^*_{min} in Fig. 2, and are used as the initial conditions for the numerically integrated outgoing solutions of the model (1). The integration of every such solution is stopped when it reaches the successive minimal value V_1. The found pairs (V_0, V_1) constitute the graph of the Poincaré mapping for selected values of the control parameter, V_{K2}^{shift} shown in Figs. 3 and 4.

Let us first focus on bursting solutions, such as the one depicted in inset (d) of Fig. 1. An example of the onto Poincaré mapping is shown in Fig. 3. Its five V-minima per burst period comprise the period-5 orbit of the mapping. A fixed point of the mapping refers to the single minimum of a periodic orbit of the model, which comes back to the same point after one cycle around the spiking manifold M_{lc}. The fixed point shown in red in Fig. 3(b) is unstable (repelling) because the absolute value of the slope of the mapping graph at the fixed point is greater than one. This unstable fixed point sets a threshold (shown in red in Fig. 3) that identifies the quiescent (below it) and the tonic spiking (above it) phases of bursting. The bursting orbit must overcome this threshold to gain an extra spike. We will show that the homoclinic bifurcations of this threshold orbit are the primary cause of complexity occurring at spike adding transitions in the interneuron model under consideration. Figure 4 shows Poincaré mappings for several values of V_{K2}^{shift}. At the beginning of the spike adding cascade the fixed point in the Poincaré mapping is stable (SP_1 in Fig. 4), corresponding to a tonic spiking orbit. The stability of the orbit is determined by whether the slope (multiplier of the fixed point) of mapping graph is less or greater than one in absolute value.

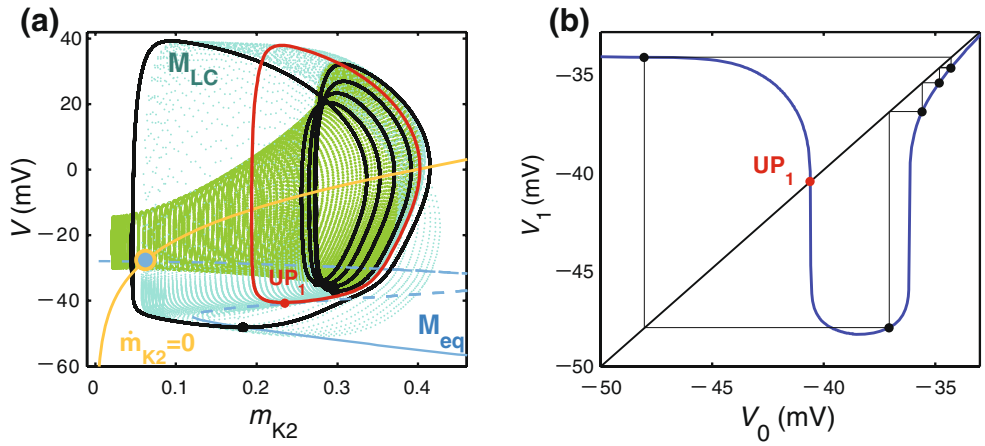

Fig. 3 Five-spike bursting orbit in the model (1) (**a**) and in the corresponding Poncaré model (**b**) at $V_{K2}^{shift} = -23$ mV. Its V-minima comprise the periodic bursting solution of the Poincaré mapping. Shown in *red* in (**a**) is a saddle periodic orbit corresponding to the unstable fixed point, UP_1 in (**b**) that sets a threshold between the quiescent and the tonic spiking sections of the mapping graph (correspondingly, *left* and *right*)

With the decrease of the control parameter the fixed point becomes unstable: the model generates bursting consisting of duplets of spikes. In the Poincaré mapping this corresponds to a stable period-2 orbit. In contrast to a typical period doubling cascade, the next transition leads to burst trains with three, not four spikes. Thus the loss of stability of the initial tonic spiking orbit leads to the onset of spike adding cascade, see Fig. 1.

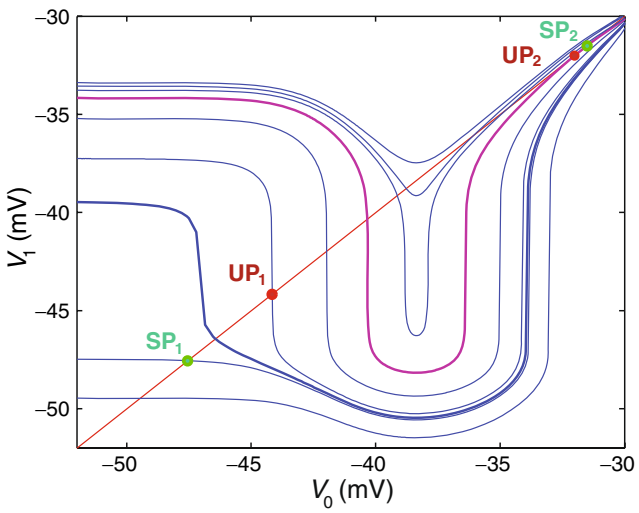

Fig. 4 V_{K2}^{shift}-parameter family of onto unimodal Poincaré mappings for the membrane potential V. A crossing point of the graph of the mapping with the 45°-line, is its fixed point corresponding to a round periodic orbit with a single V-minimum in the phase space of the model. When the shape of the mapping graph (*bold blue curve*) changes from concave up (SP_1) to concave down (UP_1), the fixed point at the inflection point changes stability, undergoing a period doubling bifurcation when its multiplier goes through -1. A tangency of the graph (*bold magenta*) with the 45°-line corresponds to the saddle-node bifurcation where two fixed points merge: stable SP_2 and unstable UP_2; here its slope equals $+1$

Figure 5(a) shows a bifurcation diagram of the Poincaré mapping. Note that each spike adding occurs within a very narrow parameter window where the model exhibits chaotic bursting. The dynamical chaos observed in these narrow windows is due to the homoclinic bifurcations of the unstable fixed point (Channell et al. 2007a). Detection of primary homoclinic orbits of the *unstable* fixed point capitalizes on a particular property of this unimodal mapping (Mira 1987; Sharkovsky et al. 1997). Namely, the primary homoclinic orbit can be detected by following a finite number of forward iterates, HO^+, of the critical point CP, of the mapping graph shown in Fig. 6. This critical point makes the mapping non-invertible, because some of the mapping points have two pre-images, i.e., one pre-image on each monotonic segments of the mapping graph. On restriction to the left from CP (decreasing segment) the unstable fixed point UP_1 is attracting for backward iterates HO^-. These backward iterates converge exponentially fast to UP_1 as time goes to $-\infty$. On other hand, UP_1 is unstable and hence the forward iterates, HO^-, of the same initial point may not converge to but jump onto UP_1 right after a finite number of steps. This number of steps defines the order of a primary homoclinic orbit, $HO^- \cup HO^+$ when it passes right through the critical point CP. An occurrence of a primary (also known as tangent) homoclinic orbit gives rise to the abundance of other homoclinics (Gavrilov and Shilnikov 1972). This phenomenon is known as a homoclinic explosion (Shilnikov et al. 1998,

2001) and leads to deterministic chaotic dynamics in a system. In order to quantify the degree of chaos in a 1D mapping $v_{n+1} = f(v_n)$, one evaluates the Lyapunov exponent $\lambda = \lim_{n\to\infty} \log(|df^n(v_o)/dv|)$. We found $\lambda \simeq 0.23$ in the first chaotic window, descends to $\simeq 0.1$ by the end of the spike adding cascade, respectively in the insets (a) and (b) of Fig. 6.

Use of the onto mapping, along with the accompanied interpretation of both local and global bifurcations of its limit sets explains the whole spike adding sequence documented in the bifurcation diagram Fig. 5(a) exceptionally well. One sees that spike adding transitions occur more frequently towards more negative values of V_{K2}^{shift} following a logarithmic scaling law (Channell et al. 2007a) illustrated in Fig. 5(b). The cascade accumulates at a critical parameter value $V_{K2}^{c} = -24.828$ mV, near which the model generates bursting with arbitrarily large number of spikes; this parameter values corresponds to the transition to tonic spiking in the interneuron model (Channell et al. 2007a).

Indeed, decreasing V_{K2}^{shift} elevates the slow nullcline $\dot{m}_{K2} = 0$ thereby bringing it closer to the spiking manifold M_{lc}. This results in the m_{K2}-component of the bursting orbit slowing down to make extra turns around the spiking manifold M_{lc}. For the mapping this means that the depolarization elevates the quiescent section (on the left from the threshold unstable fixed point) of the mapping graph so that the iterate following the quiescent point of the bursting orbit is brought up higher into the spiking section (on the right from the threshold point). This increases the number of points comprising the bursting orbit. Moreover, a further elevation of the slow nullcline can make the spiking manifold M_{lc} non-transitive for iterates throughout its spiking segment. The underlying cause is a saddle-node bifurcation leading to emergence of periodic orbits (stable and saddle)

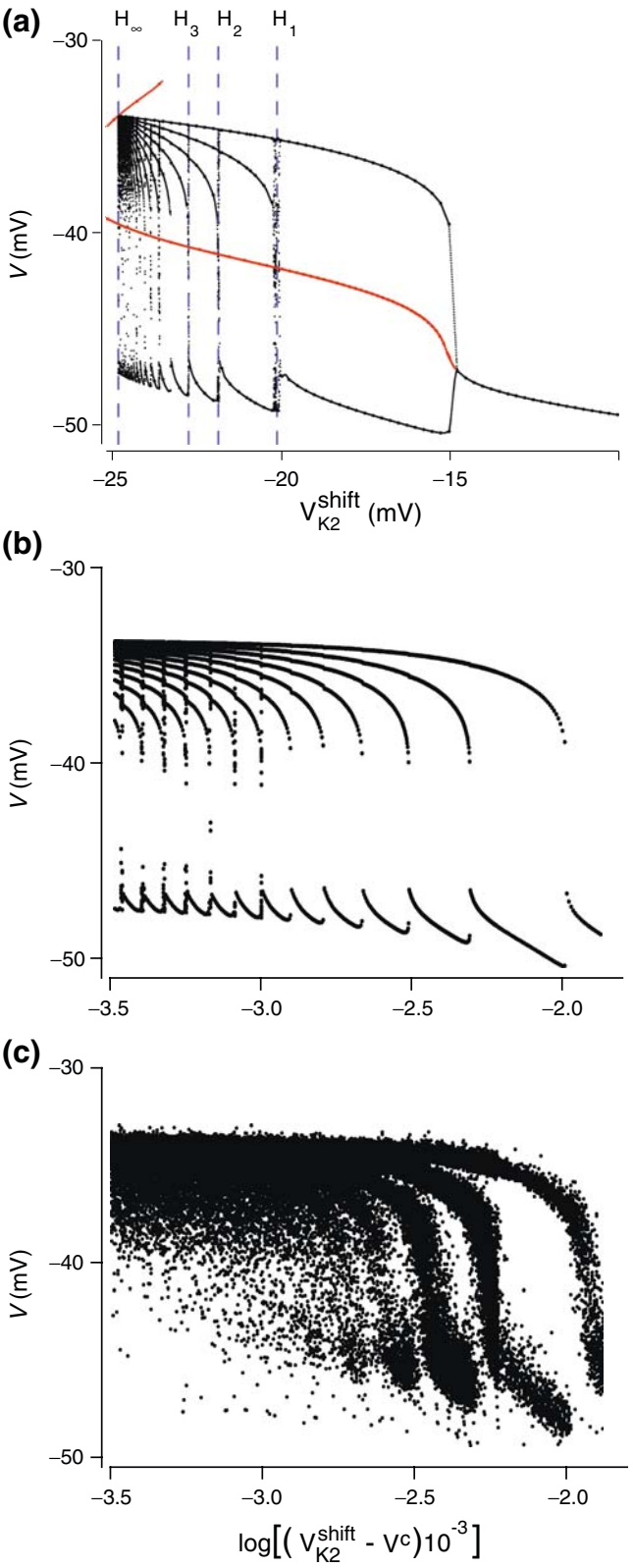

Fig. 5 Bifurcation diagrams of the model, showing the coordinates and the number of V-minima of bursting orbits plotted versus the control parameter without noise (**a** and **b**) and with noise (**c**). Panel (**a**) shows the evolution of bursting (*black*) and threshold orbits (*red*) in the onto Poincaré mapping. The *dashed vertical lines* indicate the parameter values for the first three homoclinic bifurcations. H_1 and H_∞ indicate the homoclinic bifurcations, respectively, initiating and terminating bursting in the mappings depicted in Fig. 6. Spike adding cascade intensifies as the control parameter becomes more negative towards the tonic spiking activity emerging right after the upper fold in the diagram. Panel (**b**) shows the bifurcation diagram obtained by direct numerical simulations where the minima of the bursting orbit of the interneuron model are plotted on the horizontal logarithmic scale $\log[(V_{K2}^{shift} - V^c)10^{-3}]$, where $V^c = -24.828$ is the accumulation point of the spike adding cascade; it corresponds to the terminating homoclinic bifurcation at H_∞ in panel (**a**). Panels (**b**) and (**c**) show the bifurcation diagram obtained by direct simulations of the model without noise and with added noise of the intensity $D = 10^{-7}$ nA^2/s

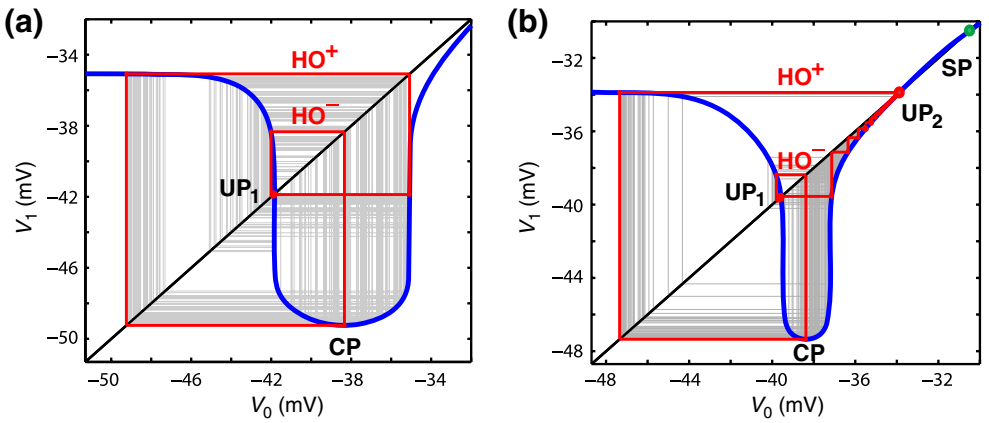

Fig. 6 Chaos in the Poincaré mapping. Grey lines show Lamerey stairs of the mapping iterations. The mapping itself is shown by blue lines. Panel (**a**) shows mapping after a primary homoclinic bifurcation of the unstable threshold fixed point, UP_1 (*red circle*) which initiates the spike adding cascade around H_1 of the bifurcation diagram of Fig. 5(a). Forward HO^+ and backward HO^- iterates of the critical points (CP) shown by *red lines* form the primary homoclinic orbit of the threshold fixed point UP_1. Panel (**b**) shows chaos due to the very heteroclinic connection between the unstable fixed points UP_1 and UP_2, which concludes the spike adding cascade at $H_\infty = V^c = -24.828$ mV in the bifurcation diagram of Fig. 5(a). The stable fixed point, SP, corresponding to the tonic spiking orbit on the manifold M_{lc}, emerges along with UP_2 through the saddle-node bifurcation (see also Fig. 4). The unstable fixed point UP_2 separates the basins of attraction of the stable tonic spiking fixed point, SP, and the bursting attractor. As soon as the critical point is taken above UP_2, bursting becomes transient towards the spiking attractor SP

on the spiking manifold.[1] The saddle-node bifurcation, also called the tangent bifurcation for one-dimensional mappings, occurs when the graph of the mapping becomes tangent to the 45° line (see Fig. 4). The newly formed fixed point separates basins of attraction of bursting and tonic spiking. This is illustrated in Fig. 7 showing coexisting spiking and bursting orbits (a) along with corresponding Poincaré mapping (b) and voltage traces (c, d).

3 Stochastic dynamics

A Gaussian noise term $\xi(t)$ was added to the first equation of the model (1) to simulate synaptic fluctuations, $C\frac{dV}{dt} = -I_{\mathrm{Na}} - I_{\mathrm{K2}} - I_{\mathrm{L}} + \xi(t)$. Normally, the fluctuations of synaptic currents occur on a time scale shorter than the characteristic time scales of a postsynaptic neuron, so that synaptic noise can be considered as δ-correlated. The autocorrelation function of the random term is given by $\langle \xi(t)\xi(t+\tau)\rangle = 2D\delta(\tau)$, where D is the noise intensity in units of nA^2/s. Our simulations showed that finite correlation times of the noise source $\xi(t)$ do not change the qualitative picture of noise effects on bursting.

One expected effect of noise on the bifurcation diagram is shown in Fig. 5(c): addition of noise lead to randomization of neuron firing so that for the given noise intensity, $D = 10^{-7}\ \mathrm{nA}^2/\mathrm{s}$, only the first four spike adding transitions can be clearly identified. Further insights concerning the effects of noise can be obtained by calculating the largest Lyapunov exponent (LE). Figure 8(a) shows the LE plotted versus $\mathrm{V}_{\mathrm{K2}}^{\mathrm{shift}}$ for several values of the noise intensity. For weak noise ($D = 10^{-9}\ \mathrm{nA}^2/\mathrm{s}$) the LE is positive in the narrow areas centered around the spike adding transitions, thus indicating an exponential divergence of the phase trajectories of the model. Outside these regions the LE is close to zero prior to a spike adding transition, but becomes negative in a narrow window right after the bifurcation. This contrasts with the purely deterministic case above, where the LE is zero everywhere except the narrow chaotic windows where it becomes positive. Thus, the effect of weak noise can be different, depending on the value of the control parameter. This reveals that noise significantly broadens the chaotic windows near the spike adding transition. With the increase of the noise intensity, regions of positive values of the LE become wider, so that eventually, starting with some critical value of the noise intensity, the LE becomes only positive regardless of $\mathrm{V}_{\mathrm{K2}}^{\mathrm{shift}}$. This is depicted in Fig. 8(b), which demonstrates clearly a non-trivial dependence of the LE versus the noise intensity: for a bifurcation parameter value in between any two spike adding transitions, the LE first decreases with the increase of noise, then reaches some minimal negative value and then increases becoming positive. For $\mathrm{V}_{\mathrm{K2}}^{\mathrm{shift}}$ near every

[1] The stable periodic orbit corresponds to tonic spiking.

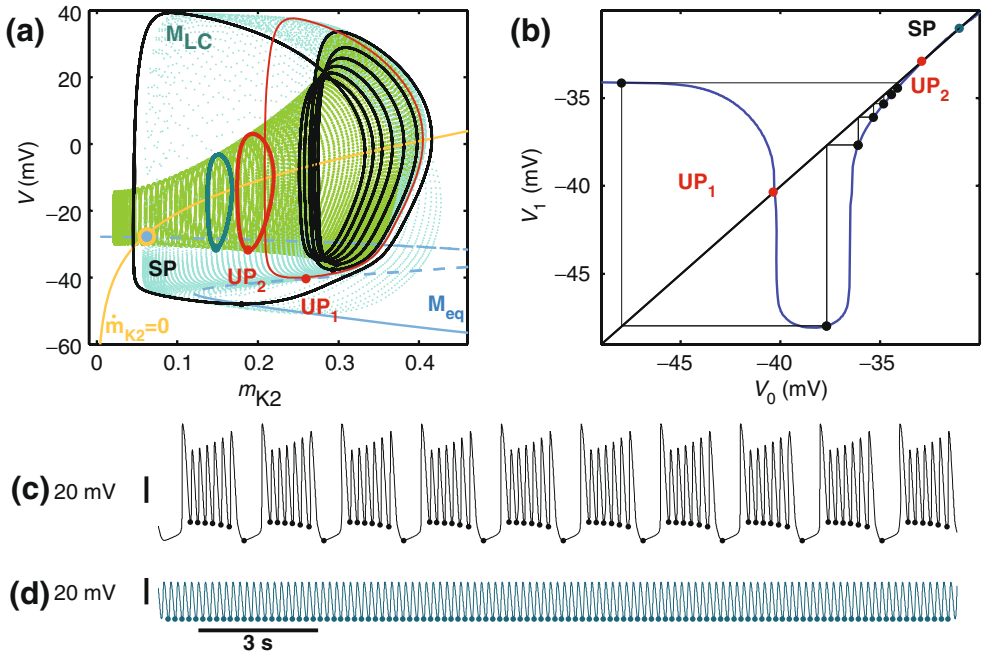

Fig. 7 Seven-spike bursting orbit (*black line*) coexisting with the tonic spiking orbit (*solid blue line*) in the phase space of the model (1) at $V_{K2}^{shift} = -24$ mV (panel (**a**)). *Red line* shows unstable threshold periodic orbits with corresponding fixed point UP_1 and UP_2. All seven V-minimum of bursting trace (panel (**c**)) and the repeating voltage minimum of the spiking trace (panel (**d**)) are the period-7 orbit and the stable fixed point (SP) in the corresponding Poincaré mapping (panel (**b**)). The stable fixed point SP emerges through a saddle-node bifurcation on the spiking manifold M_{lc} along with another unstable fixed point, UP_2 that separates the basin of attraction of tonic spiking and bursting

spike adding transition the LE remains positive and depends weakly on the noise intensity until D reaches a critical value, above which the LE starts to increase rapidly. Figure 8(c) summarizes the dependence of the LE on the control parameter and the noise intensity for several spike adding transitions. Each spike adding bifurcation gives rise to a tongue-shaped chaotic zone expanding towards higher values of the noise intensity, which is surrounded on sides by the regions of negative LE. The regions of negative values of the LE persist through a certain critical noise intensity, D_c above which the LE stays positive for an entire range of V_{K2}^{shift}. This critical noise intensity decreases as the control parameter V_{K2}^{shift} shifts towards more hyperpolarized values corresponding to the progression of the spike adding transitions.

The sign of the largest Lyapunov exponent for a neuron model can be interpreted in terms of the reliability of the neural responses to a repeated stimulation with a single realization of noise. Such stimulation protocols are routinely used in experimental neuroscience (Mainen and Sejnowski 1995). An ensemble of stimulation trials is equivalent to an ensemble of identical neurons subjected to common noise. Then, a negative LE corresponds to the convergence of the phase trajectories of the systems, which is reflected in stereotypical responses of a single neuron. In other words, neural responses to an identical realization of noise become reliable (Mainen and Sejnowski 1995). On the contrary, in a region of positive LE, neural responses to an identical realization of noise diverge (Goldobin and Pikovsky 2006). Figure 9 illustrates this interpretation of LE for the control parameter value in a middle of the period spike adding transition from five to six spikes per burst. We simulated 100 identical neurons with randomly chosen initial conditions subjected to the same realization of noise. Equivalently, such simulation can be viewed as 100 responses of a single neuron to the same segment of noise. In Fig. 9 a neuron firing a spike is represented by a dot. In the absence of noise, the LE is zero, which corresponds to a stable periodic orbit or bursting. Since neurons were started with random initial conditions, spikes are distributed randomly, as shown in Fig. 9(a). With the increase of noise the LE becomes negative. Consequently, various trials converge, demonstrating reliable neuronal responses, see Fig. 9(b). In other words, noise synchronizes a population of identical neurons (Goldobin and Pikovsky 2005). On the contrary, for larger noise the LE is positive, which leads to a randomization of neural

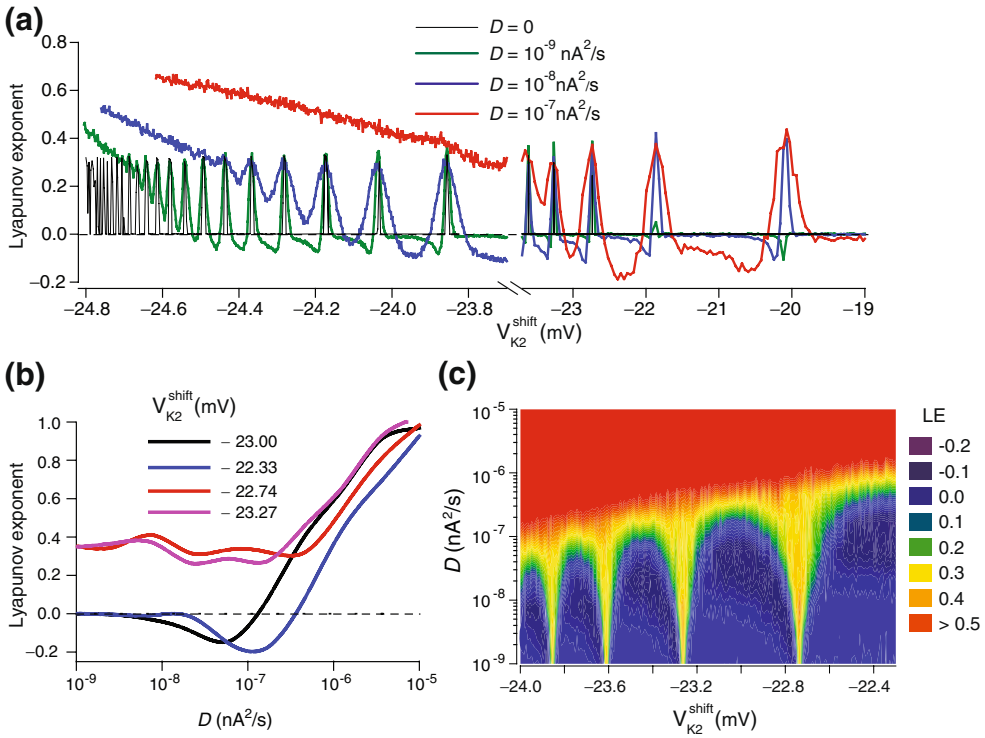

Fig. 8 (**a**) Largest Lyapunov exponent (LE) versus V_{K2}^{shift} for the indicated values of the noise intensity, D. (**b**) LE versus the noise intensity for the indicated values of the bifurcation parameter. The values of V_{K2}^{shift}, -23 and -22.33 mV are taken in the region between the successive spike adding transitions, see panels (**a**) and (**c**), while values -22.74 and -23.27 mV are picked close to the spike adding points. (**c**) LE is shown for a fragment of spike adding bifurcation sequence as a function of the bifurcation parameter V_{K2}^{shift} and the noise intensity D. The *color map* with indicated contour levels is shown on the *right*

responses, reflected in unreliable firing in response to identical noise stimulation shown in Fig. 9(c).

The transition to noisy chaos is well illustrated using a Poincaré mapping of consecutive minima of the membrane voltage traces shown in Fig. 10. In contrast to the construction of the onto Poincaré mapping described above, here such a mapping is obtained by direct simulation of a single bursting solution of the model (1) in the presence of noise. Consequently, in the noise free case, the model demonstrates a periodic bursting comprised of $n_0 = 7$ spikes per burst giving periodic orbit with 7 points in the mapping (red dots in Fig. 10(a)). Weak ($D = 10^{-9}$ nA^2/s) noise induces chaos in the model revealing the entire structure of the mapping, including the unstable branch around the unstable (threshold) fixed point. The effect of noise is clearly seen in the changes of the probability density of the consecutive voltage minima shown in Fig. 10(b). In the absence of noise the probability density, $p(V)$, is represented by a sequence of delta peaks centered at the periodic points of the mapping. Noise leads to widening of those peaks and to the appearance of non-vanishing probability near the unstable fixed point (at ≈ -40 mV) (blue line in Fig. 10(b)). Let us stress that while noise can only slightly affect the spiking part of the bursting attractor, it changes the quiescent part significantly, as indicated by a wider peak around $V = -47.0$ mV.

An alternative coarse-grained description of a spike adding sequence employs symbolic dynamics. We can

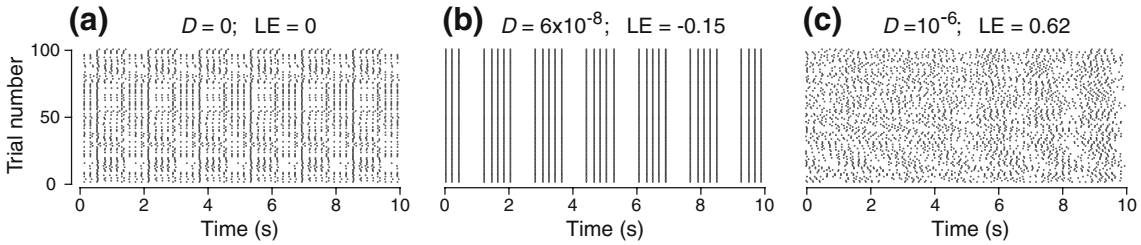

Fig. 9 Raster plots of the responses of 100 identical neuron models (1) to the same segment of noise of the indicated intensities; here $V_{K2}^{shift} = -23$ mV. Values of the largest LE are indicated for each panel

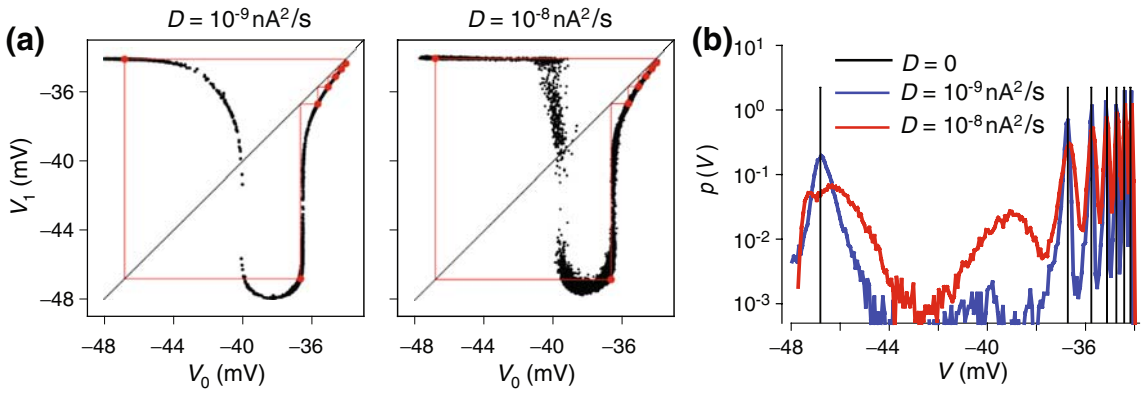

Fig. 10 (a): Poincaré mappings for $V_{K2}^{shift} = -23.84$ and the indicated values of the noise intensity. Red circles and the lines show periodic seven-spike orbit for the noiseless case. Black dots show Poincaré mapping for the stochastic model. Noise reveals the entire mapping including unstable branch crossing 45° line at a steep angle. (**b**) Probability density of consecutive minima corresponding to the Poincaré mappings in panel (**a**)

take advantage of the fact that the interspike intervals inside bursts depend weakly on the control parameter (Channell et al. 2007a) and introduce a new variable, $n(t)$, which is the number of spikes within a burst. The probability distribution, $P(n)$, of this integer is then used to characterize the coarse-grained dynamics of the system. In the stability regions, where the LE is negative, noise causes weak fluctuations of the interspike

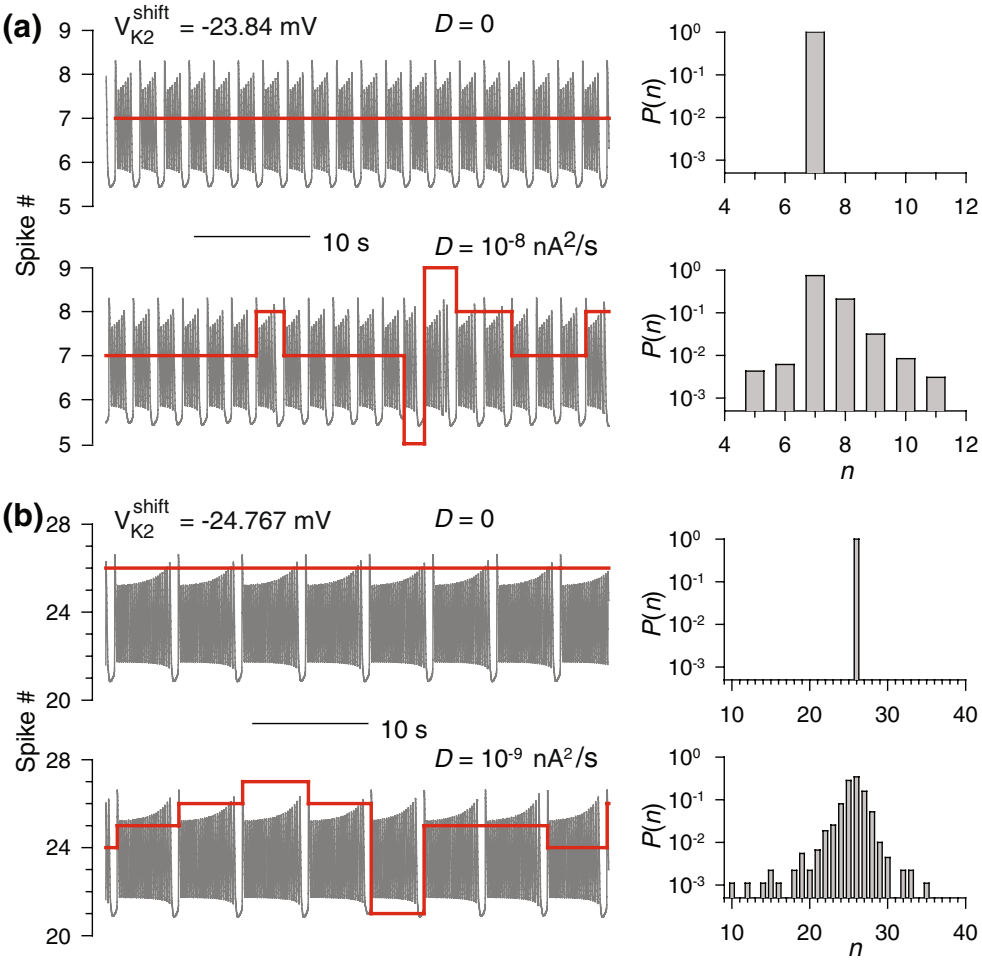

Fig. 11 (Color) Noise influence on short, of 7 spikes, and long, of 25 spikes, bursting near the spike adding transitions at (**a**) $V_{K2}^{shift} = -23.84$ mV and (**b**) $V_{K2}^{shift} = -24.767$ mV. On the *left panels* the membrane voltage V(t) is shown in *grey*, while the number of spikes, $n(t)$ (left vertical scale) is shown in *red*. *Right panels* show the corresponding distributions of the number $P(n)$ of spikes per burst for the indicated values of noise intensities

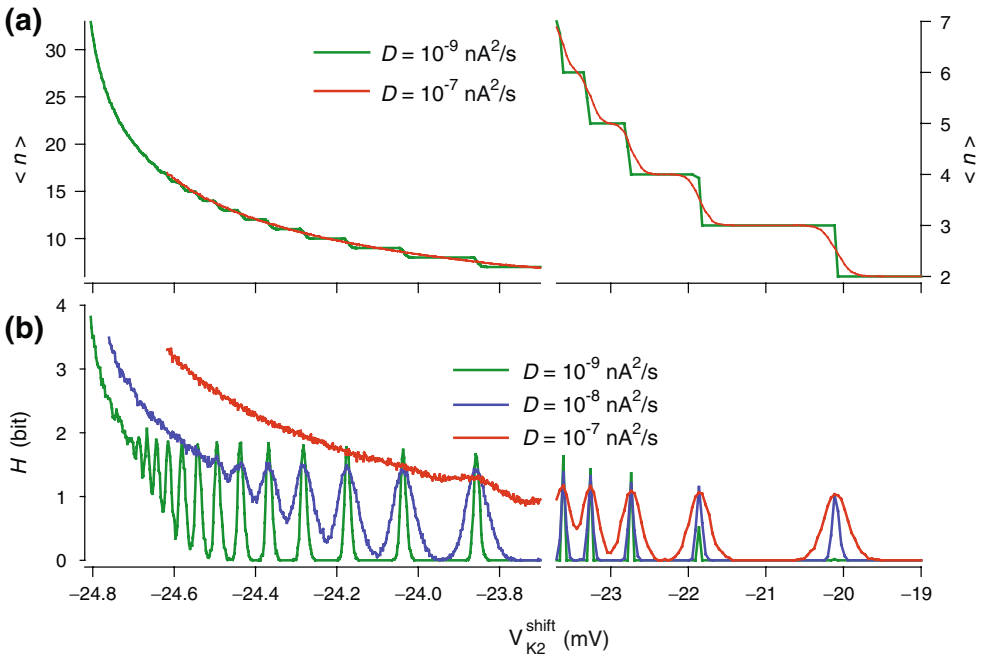

Fig. 12 (Color) (**a**) Mean number $\langle n \rangle$ of spikes per burst plotted versus the control parameter for two values of the noise intensity, $D = 10^{-9}$ nA^2 (*green line*) and $D = 10^{-7}$ nA^2 (*red line*). (**b**) Entropy (defined through Eq. (3)) against V_{K2}^{shift} for the indicated values of the noise intensity

intervals but leads to neither new spikes nor shortening bursts. As a result, the number of spikes per burst stays constant. In contrast near a spike adding transition even weak noise can change the spike number $n(t)$ so that it start jumping between several values. Figure 11 shows the membrane potential traces for V_{K2}^{shift} near two spike adding transitions for relatively short and long bursting. In the absence of noise both are periodic, which is indicated by constant $n(t) = n_0$ and the probability distributions $P(n) = \delta_{n,n_0}$, where $\delta_{i,j}$ is a Kronecker delta. With noise added, $n(t)$ varies sporadically from burst to burst thus generating the probability distribution peaked around n_0. The dependence of the mean number of spikes per burst, $\langle n \rangle$ on the control parameter shown in Fig. 12(a) reveals a staircase-like structure for weak noise: $\langle n \rangle$ is locked to constant values in the stability zones where the LE is negative, while it increases drastically fast from one step to another in the vicinity either spike adding transition. The width of the locking steps decreases with the increase of the number of spikes per burst (compare the green and red lines in Fig. 12(a)), or alternatively with the increase of the noise intensity.

The Shannon entropy of the distribution $P(n)$ can be used to quantify the stochastic bursting dynamics. For the discrete random variable $n(t)$ the entropy H is given by

$$H = -\sum_{n=1}^{M} P(n)\ \log_2 P(n), \tag{3}$$

where M is the number of attainable states of $n(t)$. Zero values of entropy reflect the absence of any variability

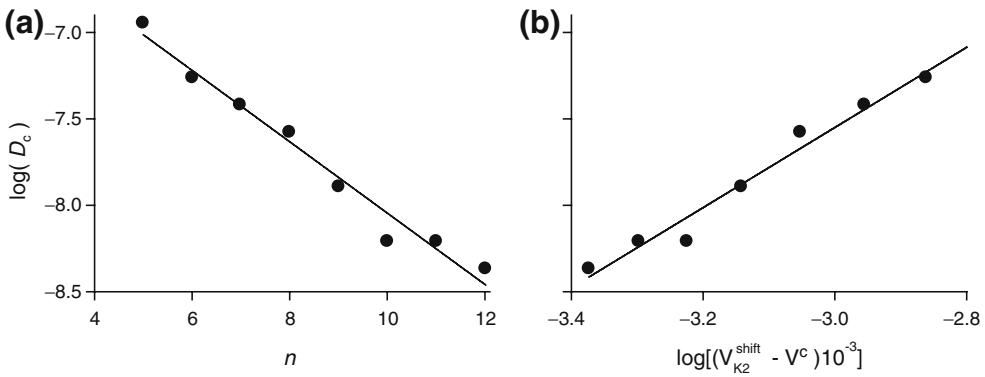

Fig. 13 Logarithmic plots of the critical noise intensity, D_c, versus the number of spike per burst (**a**) and versus $\log[(V_{K2}^{shift} - V^c)10^{-3}]$, where $V^c = -24.828$ mV is the accumulation point of the spike adding cascade. *Filled circles* indicate numerically found values; *solid lines* are the logarithmic fits

in $n(t)$. As the spike adding sequence progresses, the distances between the consecutive transitions become shorter so that the number of possible values which $n(t)$ can attain increases leading to the growth of the entropy. This is summarized in Fig. 12(b), which mimics the graph for the LE in Fig. 8. The entropy takes on maximal values at the spike adding bifurcations. In the regions between the transitions, H is 0 for weak noise. However, with the increase of the noise intensity the entropy becomes positive for the entire range of the intrinsic bifurcation parameter V_{K2}^{shift}. Figure 11(a) shows bursting with randomized spike numbers attaining seven possible values (seven bars in the probability distribution). A much higher variability is observed in Fig. 11(b); here the neuron can use up to 21 different states yielding a wider range of attainable numbers of spikes per burst. Such variability is characterized by positive values of the LE and entropy. For each spike adding transition there is a critical noise intensity, D_c, beyond which the dynamics of the model becomes chaotic in the entire region of that transition. This critical noise intensity can be estimated as follows. For each spike adding transition we determine a local minimum of the Shannon entropy at some control parameter, and then determine noise intensity for which this minimal value of H becomes positive. Such a procedure gives the critical noise intensity D_c and also the control parameter value V_{K2}^{shift} at which the minimum occurs. Figure 13 shows D_c versus the number of spike per burst, and D_c versus V_{K2}^{shift} plotted on some logarithmic scales. The critical noise intensity decreases as spike adding cascade progresses towards larger number of spikes per burst. For example, for a noise intensity D greater than 10^{-7} nA^2/s, the neuronal dynamics become globally chaotic starting with the parameter values corresponding to bursting with five spikes per burst. The same is true for D greater then 10^{-7} nA^2/s, where the LE remains positive for all values of V_{K2}^{shift} less then -23 mV. This is in agreement with the noisy bifurcation diagram represented in Fig. 5(c) showing that at $D = 10^{-7}$ nA^2/s only first four spike adding transitions are noticeable. Similarly, for D greater then 10^{-8} nA^2/s, the dynamics of the model become globally chaotic starting after the number of spikes per burst exceeding nine, and so forth.

We note that the seemingly small values of noise intensities of 10^{-9}–10^{-6} nA^2/s correspond to random synaptic current with standard deviations ranging from 0.03 to 1 pA, which are physiologically realistic perturbations for the leech heart interneurons (Cymbalyuk et al. 2002). In fact, a few pA perturbations of the leak current are enough to result in switching from bursting to tonic spiking regimes in the leach heart interneurons (Cymbalyuk et al. 2002).

4 Discussion

We have presented a case study of a mechanism of spike adding transitions in bursting dynamics of leech heart interneuron model in the presence of noise. The analysis of the deterministic model showed periodic bursting patterns except narrow chaotic islands around spike adding bifurcations. Thus, without knowing the exact location of these bifurcations in the parameter space of the model, the bursting dynamics revealed by direct numerical simulation would be judged as regular with no variability in burst pattern. This contrasts to experimental studies on bursting in isolated neurons, which showed that variability of burst durations is a rule rather than exception (Bal et al. 1988; Elson et al. 1999; Hayashi and Ishizuka 1995). We have demonstrated that the bursting dynamics in the interneuron model is highly sensitive to external random perturbations near the spike adding transitions. Furthermore, the variability of the bursting patterns increases with the progression of spike adding transitions expanding into tongue-shaped zones of noise-induced chaotic dynamics. These chaotic zones are separated by the regions of regular bursting with constant number of spikes per burst, or, equivalently, by constant burst durations as the interspike intervals within a burst does not vary much. Finally, we found a logarithmic scaling relation for the critical noise intensity beyond which dynamics of the model becomes fully chaotic within every spike adding transition parameter window.

Bursting is a manifestation of slow–fast dynamics possessing subcomponents operating at distinct time scales. Topologically, bursting is a modular activity composed of various limiting branches, corresponding to oscillatory and equilibrium states of the fast subsystem, and connected by transients between them. Due to such a complex shape of a bursting pathway, a bursting neuron responses quite unevenly to perturbations as follows from the phase resetting curve analysis (Sherwood et al., unpublished manuscript). Noise has a significant effect on bursting as well. Analytical studies have shown the effect of noise-mediated shortening of burst duration in square wave and elliptical bursters (Kuske and Baer 2002; Su et al. 2004; Pedersen and Sorensen 2007), causing, in particular, irregularity of burst patterns due to stochastic delayed loss of stability near, respectively, homoclinic and Andronov-Hopf bifurcations.

The source of instability in the interneuron model studied here is due to extended transformations of bursts through the multiple spike adding transitions. More specifically, each spike adding transition is accompanied with homoclinic bifurcations of a saddle periodic orbit that can be revealed and studied via the reduction to one-dimensional Poincaré mappings for the membrane potential. It follows from the theory of homoclinic bifurcations that the presence of a single homoclinic orbit implies a plethora of similar ones (Arnold et al. 1994; Shilnikov et al. 1998, 2001) that generate chaotic dynamics in a system. Consequently, noise may amplify transient chaos near homoclinic bifurcations (Bulsara et al. 1990; Jaeger and Kantz 1997). In the given model the winding or ordinal number of the primary homoclinic orbit increases logarithmically as the bifurcation parameter approaches the critical value, beyond which the system exhibits tonic spiking activity. Accordingly, the parameter windows of bursts with fixed numbers of spikes become progressively narrower. With noise taken into account, chaotic tongue-shaped zones of neighboring spike adding transition overlap, leading to global chaotic behavior with a positive Lyapunov exponent. The true cause of the complex dynamics at spike adding transitions in both the mapping and the model is the existence of multiple bursting orbits with weak and narrow basins of attraction. Random perturbations induce transitions among various basins of attraction, resulting in complex bursting patterns with variable numbers of spikes and thus with variable burst durations. Therefore, chaotic variability observed in the purely deterministic case only within narrow transition windows expands due to noise.

Noise-enhanced variability characterized by positive values of the Lyapunov exponent reflects unreliable neural responses to the same realization of noise (Goldobin and Pikovsky 2006). This can be contrasted to highly reliable oscillating neurons which use spike timing to encode external stimuli and thus require stereotypical responses to identical stimulus trials with a negative Lyapunov exponent (Mainen and Sejnowski 1995; Galan et al. 2008). Indeed, the leach heart interneuron is a part of a central pattern generator (CPG). CPG neuronal networks serve to sustain rhythmic activity corresponding to various oscillatory behaviors of animals such as breathing, walking and swimming. For such neurons a rich repertoire of accessible oscillatory patterns may be beneficial to achieve robustness and adaptability of a CPG network to external environmental perturbation (Rabinovich et al. 2006). In the particular example studied here, an addition of synaptic noise as small as 1 pA of standard deviation leads to a global chaotic dynamics with bursts of variable durations, which otherwise was not observed. In other words, with noise taken into account the model shows a rich repertoire of various burst patterns at a fixed value of control parameter.

In this paper we have considered a simplified version of the canonical interneuron model (Cymbalyuk et al. 2002) in presence of a synaptic noise. Following the algorithms proposed, one can reveal the structures of Poincaré return mapping for other models having noise due to stochastic cluttering of ion channels (Rowat and Elson 2004; Rowat 2007). Such voltage mappings can be determined directly from experimental voltage time series, or by using a voltage clamp technique, as described in Channell et al. (2007b). The completeness or sparseness of such mapping may vary, depending on the particular regime or on the amount of noise in a system. In the case of a sparse mapping an applied noise current can be injected to the neuron. In a too noisy case, proper statistical tests for revealing unstable periodic orbits can be used to verify whether observed bursting variability is of a low-order dynamical origin (Schiff et al. 1994; So et al. 1996; Pei and Moss 1996).

Acknowledgements The authors thank G. Cymbalyuk and R. Clewley for valuable discussions. We are grateful to anonymous reviewers for inspiring critique and useful suggestions. P.C. was supported by a fellowship through the GSU Brains and Behavior program; A.L.S. was supported by the GSU Brains and Behavior program and by the RFFI grant No 050100558. A.N. was supported in part by the Biomimetic Nanoscience and Nanotechnology program of Ohio University. I.F. was supported by the Faculty for the Future Fellowship awarded by the Schlumberger Foundation.

References

Arnold, V. I., Afraimovich, V. S., Ilyashenko, Yu. S., & Shilnikov, L. P. (1994). *Bifurcation theory. Dynamical systems. Encyclopaedia of mathematical sciences* (Vol. V). New York: Springer.

Bal, T., Nagy, F., & Moulins, M. (1988). The pyloric central pattern generator in crustacea: A set of conditional neural oscillators. *Journal of Comparative Physiology A, 163*(6), 715–727.

Belykh, V. N., Belykh, I. V., Colding-Jorgensen, M., & Mosekilde, E. (2000). Homoclinic bifurcations leading to bursting oscillations in cell models. *The European Physical Journal E—Soft Matter, 3*(3), 205–219.

Bertram, R., Butte, M. J., Kiemel, T., & Sherman, A. (1995). Topological and phenomenological classification of bursting oscillations. *Bulletin of Mathematical Biology, 57*(3), 413–439.

Bulsara, A. R., Schieve, W. C., & Jacobs, E. W. (1990). Homoclinic chaos in systems perturbed by weak langevin noise. *Physical Review A, 41*(2), 668–681.

Carelli, P. V., Reyes, M. B., Sartorelli, J. C., & Pinto, R. D. (2005). Whole cell stochastic model reproduces the irregu-

larities found in the membrane potential of bursting neurons. *Journal of Neurophysiology, 94*(2), 1169–1179.
Channell, P., Cymbalyuk, G., & Shilnikov, A. (2007a). Origin of bursting through homoclinic spike adding in a neuron model. *Physical Review Letters, 98*(13), 134101.
Channell, P., Cymbalyuk, G., & Shilnikov, A. L. (2007b). Applications of the poincare mapping technique to analysis of neuronal dynamics. *Neurocomputing, 70*, 10–12.
Chay, T. R. (1985). Chaos in a three-variable model of an excitable cell. *Physica D, 16*(2), 233–242.
Chow, C. C., & White, J. A. (1996). Spontaneous action potentials due to channel fluctuations. *Biophysical Journal, 71*(6), 3013–3021.
Clewley, R., Soto-Trevino, C., & Nadim, F. (2009). Dominant ionic mechanisms explored in spiking and bursting using local low-dimensional reductions of a biophysically realistic model neuron. *Journal of Computational Neuroscience, 26*(1), 75–90.
Cymbalyuk, G. S., & Calabrese, R. L. (2001). A model of slow plateau-like oscillations based upon the fast Na^+ current in a window mode. *Neurocomputing, 38*, 159–166.
Cymbalyuk, G. S., & Shilnikov, A. L. (2005). Coexistence of tonic spiking oscillations in a leech neuron model. *Journal of Computational Neuroscience, 18*(3), 255–263.
Cymbalyuk, G. S., Gaudry, Q., Masino, M. A., & Calabrese, R. L. (2002). Bursting in leech heart interneurons: cell-autonomous and network-based mechanisms. *Journal of Neuroscience, 22*(24), 10580–10592.
Deng, B., & Hines, G. (2002). Food chain chaos due to Shilnikov's orbit. *Chaos, 12*(3), 533–538.
Elson, R. C., Huerta, R., Abarbanel, H. D., Rabinovich, H. D., & Selverston, A. I. (1999). Dynamic control of irregular bursting in an identified neuron of an oscillatory circuit. *Journal of Neurophysiology, 82*(1), 115–122.
Elson, R. C., Selverston, A. I., Abarbanel, H. D. I., & Rabinovich, M. I. (2002). Dynamic control of irregular bursting in an identified neuron of an oscillatory circuit. *Journal of Neurophysiology, 88*, 1166–1182.
Fan, Y. S., & Holden, A. V. (1995). Bifurcations, burstings, chaos and crises in the Rose-Hindmarsh model for neuronal activity. *Chaos, Solitons and Fractals, 3*, 439–449.
Fenichel, F. (1979). Geometric singular perturbation theory for ordinary differential equations. *Journal of Differential Equations, 31*, 53–98.
Feudel, U., Neiman, A., Pei, X., Wojtenek, W., Braun, H., Huber, M., et al. (2000). Homoclinic bifurcation in a Hodgkin-Huxley model of thermally sensitive neurons. *Chaos, 10*(1), 231–239.
Galan, R. F., Ermentrout, G. B., & Urban, N. N. (2008). Optimal time scale for spike-time reliability: Theory, simulations, and experiments. *Journal of Neurophysiology, 99*(1), 277–283.
Gavrilov, N. K., & Shilnikov, L. P. (1972). On three-dimensional dynamical systems close to systems with a structurally unstable homoclinic curve. *Mathematics of the USSR, Sbornik, 17*(3), 467–485.
Goldobin, D. S., & Pikovsky, A. (2005). Synchronization and desynchronization of self-sustained oscillators by common noise. *Physical Review E, 71*, 045201.
Goldobin, D. S., & Pikovsky, A. (2006). Antireliability of noise-driven neurons. *Physical Review E, 73*, 061906.
Griffiths, R. E., & Pernarowski, M. C. (2006). Return map characterizations for a model of bursting with two slow variables. *SIAM Journal on Applied Mathematics, 66*(6), 1917–1948.
Gu, H., Yang, M., Li, L., Liu, Z., & Ren, W. (2002). Experimental observation of the stochastic bursting caused by coherence resonance in a neural pacemaker. *NeuroReport, 13*(13), 1657–1660.
Guckenheimer, J. (1996). Towards a global theory of singularly perturbed systems. *Progress in Nonlinear Differential Equations and Their Applications, 19*, 214–225.
Hayashi, H., & Ishizuka, S. (1995). Chaotic responses of the hippocampal CA3 region to a mossy fiber stimulation in vitro. *Brain Research, 686*(2), 194–206.
Hill, A. A., Lu, J., Masino, M. A., Olsen, O. H., & Calabrese, R. L. (2001). A model of a segmental oscillator in the leech heartbeat neuronal network. *Journal of Computational Neuroscience, 10*(3), 281–302.
Hodgkin, A. L., & Huxley, A. F. (1952). A quantitative description of membrane current and its application to conduction and excitation in nerve. *Journal of Physiology, 117*(4), 500–544.
Holden, A. V., & Fan, Y. S. (1992). From simple to simple bursting oscillatory behaviour via intermittent chaos in the Rose-Hindmarsh model for neuronal activity. *Chaos, Solitons and Fractals, 2*, 349–269.
Izhikevich, E. M. (2000). Neural excitability, spiking and bursting. *International Journal of Bifurcation and Chaos, 10*, 1171–1266.
Izhikevich, E. M. (2007). *Dynamical systems in neuroscience. The geometry of excitability and bursting*. Cambridge: MIT.
Jaeger, L., & Kantz, H. (1997). Homoclinic tangencies and non-normal jacobians—effects of noise in nonhyperbolic chaotic systems. *Physica D, 105*(1–3), 79–96.
Jones, C. K. R. T., & Kopell, N. (1994). Tracking invariant-manifolds with differential forms in singularly perturbed systems. *Journal of Differential Equations, 108*(1), 64–88.
Kramer M., Traub, R. D., & Kopell, N. J. (2008) New dynamics in cerebellar purkinje cells: Torus canards. *Physics Review Letters, 101*, 068103.
Kopell, N. (1988). Toward a theory of modelling central pattern generators. In A. H., Cohen, S., Rossingol, & S., Grillner (Eds.), *Neural control of rhythmic movements in vertebrates* (pp. 1–20). New York: Wiley.
Kuske, R., & Baer, S. M. (2002). Asymptotic analysis of noise sensitivity in a neuronal burster. *Bulletin of Mathematical Biology, 64*(3), 447–481.
Mainen, Z. F., & Sejnowski, T. J. (1995). Reliability of spike timing in neocortical neurons. *Science, 268*(5216), 1503–1506.
Manwani, A., & Koch, C. (1999). Detecting and estimating signals in noisy cable structure, I: Neuronal noise sources. *Neural Computation, 11*(8), 1797–1829.
Marder, E., & Calabrese, R. L. (1996). Principles of rhythmic motor pattern generation. *Physiological Reviews, 76*(3), 687–717.
Medvedev, G. M. (2005). Reduction of a model of an excitable cell to a one-dimensional map. *Physica D, 202*(1–2), 87–106.
Medvedev, G. M. (2006). Transition to bursting via deterministic chaos. *Physical Review Letters, 97*, 048102.
Mira, C. (1987). *Chaotic dynamics from the one-dimensional endomorphism to the two-dimensional diffeomorphism*. Singapore: World Scientific.
Pedersen, M. G., & Sorensen, M. P. (2007). The effect of noise of β-cell burst period. *SIAM Journal on Applied Mathematics, 67*, 530–542.
Pei, X., & Moss, F. (1996). Characterization of low-dimensional dynamics in the crayfish caudal photoreceptor. *Nature, 379*(6566), 618–621.
Pontryagin, L. S., & Rodygin, L. V. (1960). Periodic solution of a system of ordinary differential equations with a small parameter in the terms containing derivatives. *Soviet Mathematics. Doklady, 1*, 611–661.

Rabinovich, M. I., Varona, P., Silverston, A. L., & Abarbanel, H. D. (2006). Dynamics principles in neuroscience. *Reviews of Modern Physics, 78*(4), 1213–1265.

Rinzel, J. (1985). Bursting oscillations in an excitable membrane model. *Lecture Notes in Mathematics, 1151*, 304–316.

Rinzel, J., & Ermentrout, B. (1998). Analysis of neural excitability and oscillations. In C., Koch & I., Segev (Eds.), *Computational neuroscience* (pp. 135–169). Cambridge: MIT.

Rinzel, J., & Wang, X. J. (1995). Oscillatory and bursting properties of neurons. In M. Arbib (Ed.), *The handbook of brain theory and neural networks* (pp. 686–691). Cambridge: MIT.

Rowat, P. (2007). Interspike interval statistics in the stochastic Hodgkin-Huxley model: Coexistence of gamma frequency bursts and highly irregular firing. *Neural Computation, 19*(5), 1215–1250.

Rowat, P. F., & Elson, R. C. (2004). State-dependent effects of Na channel noise on neuronal burst generation. *Journal of Computational Neuroscience, 16*(2), 87–112.

Schiff, S. J., Jerger, K., Duong, D. H., Chang, T., Spano, M. L., & Ditto, W. L. (1994). Controlling chaos in the brain. *Nature, 370*(6491), 615–620.

Sharkovsky, A. N., Kolyada, S. F., Sivak, A. G., & Fedorenko, V. V. (1997). *Dynamics of one-dimensional maps. Mathematics and its applications* (Vol. 407). Dordrecht: Kluwer.

Shilnikov, A. L. (1993). On bifurcations of the Lorenz attractor in the Shimizu-Morioka model. *Physica D, 62*(1–4), 338–346.

Shilnikov, A., & Cymbalyuk, G. (2004). Homoclinic saddle-node orbit bifurcations en a route between tonic spiking and bursting in neuron models, invited paper. *Regular & Chaotic Dynamics, 9*, 281–297.

Shilnikov, A. L., Calabrese, R. L., & Cymbalyuk, G. (2005). Mechanism of bistability: Tonic spiking and bursting in a neuron model. *Physical Review E, 71*, 056214.

Shilnikov, A. L., & Cymbalyuk, G. (2005). Transition between tonic spiking and bursting in a neuron model via the blue-sky catastrophe. *Physical Review Letters, 94*(4), 048101.

Shilnikov, A. L., & Kolomiets, M. L. (2008). Methods of the qualitative theory for the Hindmarsh-Rose model: A case study. A tutorial. *International Journal of Bifurcation and Chaos, 18*(7), 1–32.

Shilnikov, A. L., & Rulkov, N. F. (2003). Origin of chaos in a two-dimensional map modelling spiking-bursting neural activity. *International Journal of Bifurcation and Chaos, 13*(11), 3325–3340.

Shilnikov, A. L., & Rulkov, N. F. (2004). Subthreshold oscillations in a map-based neuron model. *Physics Letters A, 328*(2–3), 177–184.

Shilnikov, L. P., Shilnikov, A. L., Turaev, D., & Chua, L. O. (1998, 2001). *Methods of qualitative theory in nonlinear dynamics* (Vols. 1 and 2). Singapore: World Scientific.

So, P., Ott, E., Schiff, S. J., Kaplan, D. T., Sauer, T., & Grebogi, C. (1996). Detecting unstable periodic orbits in chaotic experimental data. *Physical Review Letters, 76*(25), 4705–4708.

Steriade, M., Jones, E. G., & Llinas, R. R. (1990). *Thalamic oscillations and signaling*. New York: Wiley.

Steriade, M., McCormick, D. A., & Sejnowski, T. J. (1993). Thalamocortical oscillations in the sleeping and aroused brain. *Science, 262*(5134), 679–685.

Su, J., Rubin, J., & Terman, D. (2004). Effects of noise on elliptic bursters. *Nonlinearity, 17*, 13300157.

Terman, D. (1991). Chaotic spikes arising from a model of bursting in excitable membranes. *SIAM Journal on Applied Mathematics, 51*(5), 1418–1450.

Terman, D. (1992). The transition from bursting to continuous spiking in excitable membrane models. *Journal of Nonliear Science, 2*(2), 135–182.

Tikhonov, A. N. (1948). On the dependence of solutions of differential equations from a small parameter. *Matemati(c)eskij Sbornik, 22*(64), 193–204.

Wang, X. J. (1993). Genesis of bursting oscillations in the Hindmarsh-Rose model and homoclinicity to a chaotic saddle. *Physica D, 62*(1–4), 263–274.

Yang, Z., Qishao, L., & Li, L. (2006). The genesis of period-adding bursting without bursting-chaos in the Chay model. *Chaos, Solitons and Fractals, 27*(3), 689–697.